

Construction of two-qubit logical gates by transmon qubits in a three-dimensional cavity

Han Cai(蔡涵), Qi-Chun Liu(刘其春), Chang-Hao Zhao(赵昌昊), Ying-Shan Zhang(张颖珊), Jian-She Liu(刘建设), Wei Chen(陈炜)

Citation: Chin. Phys. B . 2018, 27(8): 084207. **doi:** 10.1088/1674-1056/27/8/084207

Journal homepage: http://cpb.iphy.ac.cn; http://iopscience.iop.org/cpb

What follows is a list of articles you may be interested in

Scattering of a single photon in a one-dimensional coupled resonator waveguide with a Λ-type emitter assisted by an additional cavity

Ming-Xia Li(厉鸣夏), Jie Yang(杨洁), Gong-Wei Lin(林功伟), Yue-Ping Niu(钮月萍), Shang-Qing Gong(龚尚庆)
Chin. Phys. B . 2018, 27(5): 054206. **doi:** 10.1088/1674-1056/27/5/054206

Broadrange tunable slow and fast light in quantum dot photonic crystal structure

Alireza Lotfian, Reza Yadipour, Hamed Baghban
Chin. Phys. B . 2017, 26(12): 124207. **doi:** 10.1088/1674-1056/26/12/124207

Resonantly driven exciton Rabi oscillation in single quantum dots emitting at 1300 nm

Yong-Zhou Xue(薛永洲), Ze-Sheng Chen(陈泽升), Hai-Qiao Ni(倪海桥), Zhi-Chuan Niu(牛智川), De-Sheng Jiang(江德生), Xiu-Ming Dou(窦秀明), Bao-Quan Sun(孙宝权)
Chin. Phys. B . 2017, 26(8): 084202. **doi:** 10.1088/1674-1056/26/8/084202

Analytical solutions for a doubly driven two-level atom

Jin-Yun Liu(刘晋允), Feng-Dong Jia(贾凤东), Xiao-Kang Li(李晓康), Shuang-Fei Lv(吕双飞), Xiang-Yuan Xu(许祥源), Ping Xue(薛平), Zhi-Ping Zhong(钟志萍)
Chin. Phys. B . 2017, 26(7): 074203. **doi:** 10.1088/1674-1056/26/7/074203

Algebraic and group treatments to nonlinear displaced number statesand their nonclassicality features: A new approach

N Asili Firouzabadi, M K Tavassoly, M J Faghihi
Chin. Phys. B . 2015, 24(6): 064204. **doi:** 10.1088/1674-1056/24/6/064204

Construction of two-qubit logical gates by transmon qubits in a three-dimensional cavity*

Han Cai(蔡涵), Qi-Chun Liu(刘其春), Chang-Hao Zhao(赵昌昊), Ying-Shan Zhang(张颖珊), Jian-She Liu(刘建设), and Wei Chen(陈炜)†

Tsinghua National Laboratory for Information Science and Technology, Department of Microelectronics and Nanoelectronics, Institute of Microelectronics, Tsinghua University, Beijing 100084, *China*

(Received 12 March 2018; revised manuscript received 17 April 2018; published online 25 July 2018)

We report the implementation of qubit–qubit coupling in a three-dimensional (3D) cavity, using the exchange of virtual photons, to realize logical operations. We measure single photon and multi-photon transitions in this qubit–qubit coupling system and obtain its energy avoided-crossing spectrum. With ac-Stark effect, fast control of the qubits is achieved to tune the effective coupling on and off and the state-swap gate $\sqrt{\text{SWAP}}$ is successfully constructed. Moreover, using two-photon transition between the ground state and doubly excited states, a kind of two-photon Rabi-like oscillation is observed. A quarter period of this oscillation corresponds to the logical gate $\sqrt{\text{bSWAP}}$, which is used for generating Bell states. $\sqrt{\text{bSWAP}}$ and $\sqrt{\text{iSWAP}}$ are the foundations of future preparation of two-qubit Bell states and realization of CNOT gate.

Keywords: 3D transmon qubit, qubit–qubit coupling, coherent state exchange, Rabi-like oscillation

PACS: 42.50.Ct, 03.67.Lx, 74.78.Na, 85.25.Hv **DOI:** 10.1088/1674-1056/27/8/084207

1. Introduction

Superconducting circuits are promising candidates for constructing a quantum computer, and superconducting quantum computation has witnessed fast development.[1,2] Recent progress in superconducting quantum computation concerns the demonstration of high-fidelity single-qubit quantum gates,[3,4] high-fidelity qubit measurements,[5–10] and realization of basic quantum algorithms.[11–15] However, in order to realize quantum computing, the operation of two qubits logical gates is necessary. Theoretically, single-qubit gates and two-qubit gates are all the ingredients needed for quantum computation. Multi-qubit quantum gates based on phase qubit[16–21] have been reported.

Compared to other superconducting qubits, three-dimensional (3D) superconducting transmon qubit has long coherence time. However, it is difficult to realize multi-qubit coupling and perform relevant logical gate operation. In this paper, we studied the coupling between two transmon qubits in a 3D cavity. When two qubits are in resonance, iSWAP gate and $\sqrt{\text{iSWAP}}$ gate are constructed in $|01\rangle \leftrightarrow |10\rangle$ state-swap process. When two qubits are off resonance, bSWAP gate and $\sqrt{\text{bSWAP}}$ gate are constructed by using the two-photon absorption process from the ground state $|00\rangle$ to the double-excited state $|11\rangle$. As a comparison, the elapsed time of $\sqrt{\text{iSWAP}}$ gate based on resonant qubits can be controlled by tuning their coupling strength. $\sqrt{\text{bSWAP}}$ gate is based on non-resonant qubits, therefore it cannot be restricted through qubit frequencies. Besides, $\sqrt{\text{bSWAP}}$ gate requires longer elapsed time since it comprises two-photon process.

2. Qubit–qubit coupling system

Qubits can share either tunable coupling or fixed coupling. In tunable coupling geometry, the coupling path between different qubits can be switched on and off. In fixed coupling geometry, the coupling path always exists between qubits, while the coupling strength can be adjusted by tuning the qubits on or off resonance. Both coupling types enable the realization of two-qubit quantum gate.

The experiment is performed at cryogenic dilution refrigerator with a base temperature of 10 mK. Figure 1 is the wiring diagram and circuit components. A 3D copper microwave cavity is used to couple two independent transmon qubit chips. The two qubits are mounted in parallel in the middle of the cavity, as shown in Fig. 1(b). The 3D cavity has a fundamental eigen-frequency of $\omega_c/2\pi = 7.9411$ GHz and a loaded quality factor $Q_L \approx 15000$. The fabrication process of qubits is based on double angle evaporation and the area of Al/AlO_x/Al Josephson junction is about 210 nm × 150 nm. The junction structures of these two transmon qubits are SQUID-type and single-junction-type, respectively, which are marked as Q1 and Q2. SQUID-type qubit has two junctions in a loop whose frequency is tunable. We can vary the external magnetic field to tune the qubit's energy spectrum. Besides, the method of single sideband modulation is used to perform two-qubit gates,

*Project supported by the National Basic Research and Development Program of China (Grant No. 2011CBA00304), the National Natural Science Foundation of China (Grant Nos. 60836001 and 61174084), and the Tsinghua University Initiative Scientific Research Program, China (Grant No. 20131089314).

†Corresponding author. E-mail: weichen@tsinghua.edu.cn

© 2018 Chinese Physical Society and IOP Publishing Ltd

allowing fast-tuning of microwave source frequency to match the qubit frequency. The technique of ac-Stark shift has also been applied to the measurement to realize fast-tuning of the qubit transition frequency and swapping two qubits states for performing logical gate.

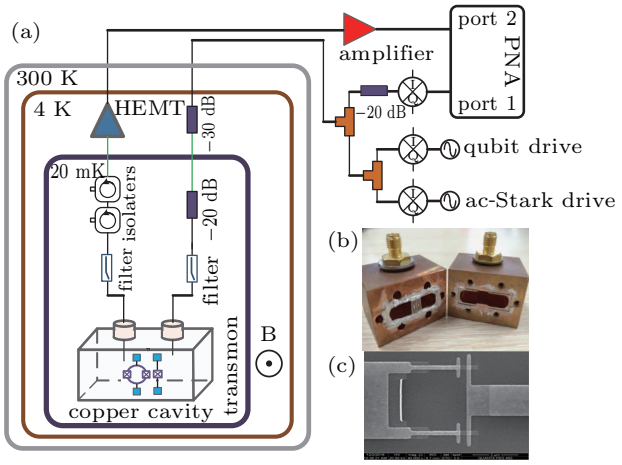


Fig. 1. (color online) Schematic diagram of the experimental system and 3D transmon sample. (a) Experimental setup; (b) 3D cavity; and (c) SQUID-type transmon sample.

The two qubits in the coupling system are coupled to each other by 3D cavity with virtual photon process. The-single-junction-type qubit (Q2) couples to the cavity, and by varying the external magnetic flux, the SQUID-type qubit (Q1) is tuned into resonance with the cavity, which means these two qubits are in resonance through the cavity. The effective Hamiltonian of this system can be written as follows:[22]

$$\begin{aligned} H &= \frac{\hbar}{2}\omega^{(1)}\sigma_z^{(1)} + \frac{\hbar}{2}\omega^{(2)}\sigma_z^{(2)} \\ &+ \hbar\left(\omega_c + \chi^{(1)}\sigma_z^{(1)} + \chi^{(2)}\sigma_z^{(2)}\right)a^\dagger a \\ &+ \hbar J\left(\sigma_-^{(1)}\sigma_+^{(2)} + \sigma_-^{(2)}\sigma_+^{(1)}\right), \end{aligned} \tag{1}$$

where $\chi^{(1)}$ and $\chi^{(2)}$ denote the qubit-state-dependent cavity frequency shift and J is the effective coupling strength of the two qubits. The interaction strength is controlled by tuning SQUID-type qubit energy level. By applying an external magnetic flux, the Q1 transition frequency is tuned close to Q2, and then the energy spectrum of this coupling system is measured.

Figure 2 shows the energy spectrum of the quit–qubit coupling system at two different magnetic bias currents. Because of the detuning between two qubits in these two magnetic bias currents, the qubit–qubit coherent interaction strength is weak and the energy spectrum of each qubit can be distinguished. Comparing the red and blue curves, it shows that three peaks are fixed in the varying magnetic field. These fixed peaks correspond to the transition frequencies of Q2: $f_{01}^{(2)} = 7.1523$ GHz, $f_{02}^{(2)}/2 = 6.9887$ GHz, $f_{03}^{(2)}/3 = 6.8250$ GHz, and the energy level anharmonicity $\alpha^{(2)} = 327.2$ MHz. The transition frequencies of Q1 are varying with the bias magnetic field. When magnetic bias currents are 18.15 mA and 18.55 mA, the transition frequencies are $f_{01}^{(1)} = 7.0570$ GHz and $f_{01}^{(1)} = 6.9541$ GHz, respectively. The anharmonicity is $\alpha^{(1)} = 276.0$ MHz. The spectral peak of the two photons transition $|00\rangle \rightarrow |11\rangle$ is also observed in the coupling system spectrum which corresponds to the transition frequency $(f_{01}^{(1)} + f_{01}^{(2)})/2$ and can be adjusted by tuning the Q1 frequency.

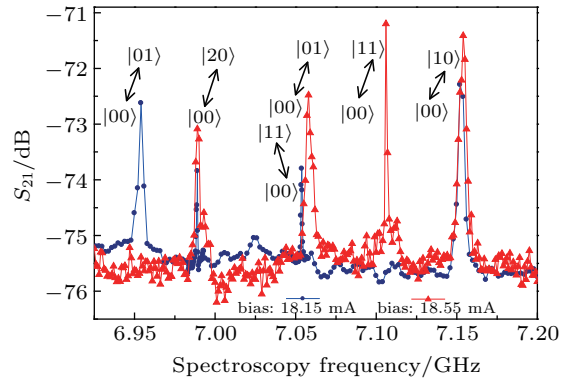


Fig. 2. (color online) Energy spectrum of qubit–qubit coupling system at 18.15 mA (blue line) and 18.55 mA (red line) magnetic bias current.

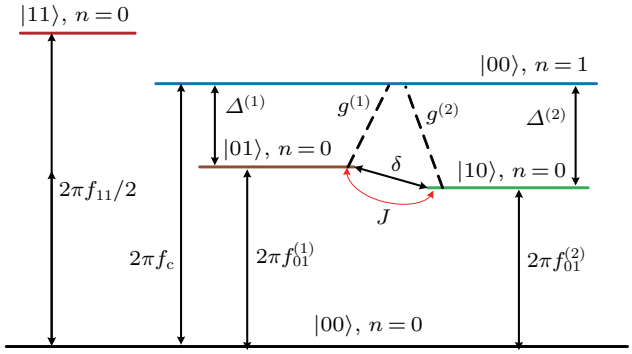


Fig. 3. (color online) The schematic energy levels of two qubits coupled by virtual photon via cavity.

In this coupling system, the two qubits interact by virtual exchange of photons via the cavity. If qubit Q1 is tuned into resonance with qubit Q2, the excited state in a qubit will generate a virtual photon in the cavity, transferring the excitation to the other qubit, as shown in Fig. 3, and the effective strength of swap interaction is $J = g^{(1)}g^{(2)}(1/\Delta^{(1)} + 1/\Delta^{(2)})/2$. By varying the external magnetic bias current, when the qubits are near resonance, an avoided crossing is observed in the energy spectrum, which reflects the exchange of the coherent state between two qubits by the virtual photon interaction.[23] If the two qubits are far detuned $\left|\omega^{(1)} - \omega^{(2)}\right| \gg J$, the swap interaction will be effectively suppressed and the two qubits are decoupled.

In order to measure the maximum coupling strength J between two qubits via cavity, we vary the magnetic bias current and tune the two qubits near resonance. Swap interaction leads

to the splitting in two-qubit energy spectrum, where the splitting width should be $2J$. When the transition frequencies of Q1 and Q2 are $f_{01}^{(1)} = f_{01}^{(2)} = 7.1523$ GHz, the detuning between qubits and cavity are $\Delta^{(1)}/2\pi = \Delta^{(2)}/2\pi = 0.8357$ GHz. By varying the external magnetic field and scanning the transmission S_{21} of qubit and cavity coupling system, the spectrum of vacuum Rabi splitting is obtained and the distance between the splitting peaks is twice the coupling strength between the qubit and the cavity, $2g$. Therefore, the qubit-cavity coupling strength is $g^{(1)} \approx 2\pi \times 120$ MHz. Since Q1 and Q2 have the same qubit-cavity coupling capacitance, they should have similar qubit-cavity coupling strength, $g^{(2)} \approx 2\pi \times 120$ MHz. Then the effective qubit–qubit coupling strength can be theoretically calculated: $J = 2\pi \times 17.2$ MHz. From the experimental results shown in Fig. 4, the distance of the splitting is 29.0 MHz, which reflects the value of the effective qubit–qubit coupling strength in resonance $J = 2\pi \times 14.5$ MHz, slightly less than the calculated value $2\pi \times 17.2$ MHz. It may be due to the error in vacuum Rabi splitting measurement, or that the qubit's anharmonicity is not large enough to make a two-level system approximation, thus higher levels have influence on the qubit–qubit coupling.

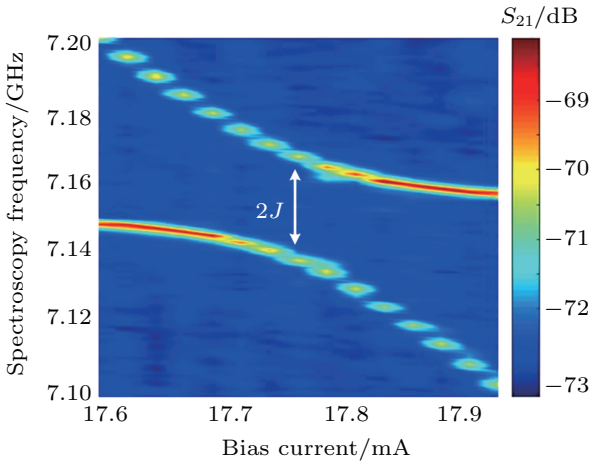


Fig. 4. (color online) Spectroscopy of avoided-crossing.

When the transition frequencies of these two qubits are far detuned, the interaction will be weak enough. Therefore, the qubits can be characterized separately. In order to calibrate the intrinsic properties of each qubit, the transition frequency of Q1 is tuned to $f_{01}^{(1)} = 8.932$ GHz, thus the detuning between the two qubits is 1.78 GHz. Then, the decay features have also been measured, including Rabi oscillation, energy relaxation, and spin echo. The coherence times are measured to be $T_{\text{Rabi}}^{(1)} = 1.5$ μs, $T_1^{(1)} = 1.6$ μs, $T_{\text{echo}}^{(1)} = 0.7$ μs, $T_{\text{Rabi}}^{(2)} = 1.8$ μs, $T_1^{(2)} = 1.3$ μs, and $T_{\text{echo}}^{(2)} = 2.8$ μs. The comparison of the coherence times of the two qubits shows that these two qubits have close energy relaxation times, but the dephasing times are quite different. Because the SQUID-type qubit is sensitive to the magnetic flux noise while the magnetic noise has almost no influence on the singe-junction-type qubit, the Q1 dephasing time is shorter than Q2, $T_{\text{echo}}^{(1)} < T_{\text{echo}}^{(2)}$.

3. Realizing $\sqrt{\text{iSWAP}}$ and $\sqrt{\text{bSWAP}}$ gates

Using the virtual photon process in qubit–qubit coupling system, two-qubit logical gates can be constructed, such as state-swap gates iSWAP and $\sqrt{\text{iSWAP}}$.[24] By adjusting the qubit–qubit detuning, the effective qubit–qubit coupling strength J can be controlled. In order to shift the effective qubit transition frequencies, ac-Stark effect is applied to the coupling system to change the number of photons in the cavity. The ac-Stark shift of the qubit frequencies can be precisely controlled by the qubit–qubit detuning and the mean photon numbers in the cavity. Therefore, ac-Stark effect is used to tune the qubit frequency and then construct the logical $\sqrt{\text{iSWAP}}$ gate.

In the experiment of qubit–qubit state swap, a π pulse is applied to one qubit to generate the system state $|01\rangle$ or $|10\rangle$, followed by a Stark pulse to the coupling system for tuning the two qubit frequencies. Different Stark pulses will result in different frequency shifts for Q1 and Q2. Due to the different detuning between the Stark drive field and each qubit, $\Delta_{\text{Stark}}^{(1)} \neq \Delta_{\text{Stark}}^{(2)}$, Q1 and Q2 have different frequency shifts, then the qubit–qubit detuning δ will vary. By changing the power and frequency of the Stark drive field, the qubit–qubit detuning δ is tuned to pull qubits into resonance. Thus, the state swap between $|01\rangle$ and $|10\rangle$ will be realized. Here, the magnetic bias current is set as 18.05 mA, so that the Q1 frequency is $f_{01}^{(1)} = 7.0815$ GHz. The detuning between two qubits is $\delta/2\pi = f_{01}^{(2)} - f_{01}^{(1)} = 70.8$ MHz, which means the interaction between the qubits is weak enough that we can operate separately on these two qubits. The initial state of the system is $|00\rangle$. A π pulse is applied to Q2 to produce the state $|10\rangle$. After that, the Stark shift is induced to bring the qubits near resonance and then the length of driving pulse is scanned. The Stark drive field frequency is $f_{\text{Stark}} = 7.350$ GHz and the power is -12 dBm. The detuning between the Stark drive field and the qubits is $\Delta_{\text{Stark}}^{(1)}/2\pi = 268.5$ MHz and $\Delta_{\text{Stark}}^{(2)}/2\pi = 197.7$ MHz, respectively. From the curve in Fig. 5(a), with the variation of the Stark pulse length, the system state periodically oscillates between $|01\rangle$ and $|10\rangle$, which represents the state transfer from one qubit to another. The swap frequency corresponds to the effective coupling strength and the Stark pulse length of a quarter swap period corresponds to a $\sqrt{\text{iSWAP}}$ gate operation. The decay of the amplitude of the oscillation curve corresponds to the decoherence of the system states. When both qubits relax, the process of swap states cannot be detected any more.

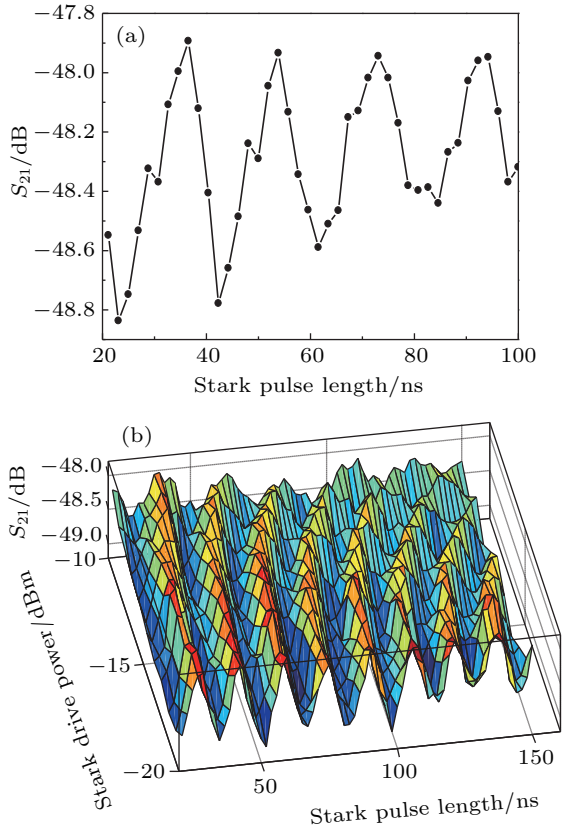


Fig. 5. (color online) Coherent states exchange between qubits. (a) Stark drive power is −12 dBm and (b) Stark drive power varies.

Figure 5(b) is the repeated experiments to observe the characters of two-qubit state swap at different Stark pulse powers. It shows that the state swap oscillation will be altered with the variation of the Stark pulse power. This phenomenon corresponds to the change of qubit–qubit detuning δ caused by the Stark pulse power, thus resulting in the change of the state swap frequency. For further discussion, each oscillation frequency in Fig. 5 is extracted and we get the relationship between the state swap frequency and the Stark pulse power, as shown in Fig. 6. It shows that the frequency of the two-qubit state swap will decrease as the Stark pulse power increases. It corresponds to the qubit-Stark drive field detuning $\Delta^{(1)}_{\text{Stark}} > \Delta^{(2)}_{\text{Stark}} >$. Under the effect of the Stark drive field, the frequency shift of Q2 is larger than that of Q1 and both of them are shifted to lower frequencies. Because $f^{(2)}_{01} > f^{(1)}_{01}$, the detuning between these two qubit will decrease, which results in the reduced frequency of the state swap. By varying the Stark pulse power, the detuning of the two qubits δ is minimized to $2\pi \times 37.5$ MHz, which is close to the energy avoided crossing splitting $2J = 2\pi \times 29$ MHz.

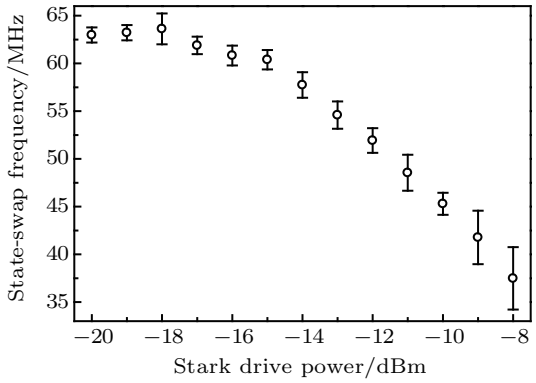


Fig. 6. The variation of state-swap frequency as the Stark drive power increases.

According to the spectrum in Fig. 2, the process of the two-photon transition $|00\rangle \leftrightarrow |11\rangle$ is observed. Using this two-photon transition, we can construct two-qubit logical gate $\sqrt{\text{bSWAP}}$ which can be used to generate two-qubit Bell state $(|00\rangle + e^{i\varphi}|11\rangle)/\sqrt{2}$. Here, the magnetic bias current is set at 18.05 mA. Applying a driving field with driving frequency near $(f^{(1)}_{01} + f^{(2)}_{01})/2$ to the qubit–qubit coupling system, the ground state and the doubly excited state will be coupled. By spectrum measurement, the transition frequency of two-photon process $|00\rangle \rightarrow |11\rangle$ is obtained, which is 7.1186 GHz. Comparing the experimental results to the theoretical value $(f^{(1)}_{01} + f^{(2)}_{01})/2$, the difference is about 1.7 MHz. Under the rotating wave approximation, when the driving field frequency is equal to the two-photon transition frequency, the qubit–qubit coupling system will undergo Rabi-like oscillation between the ground state $|00\rangle$ and the doubly excited states $|11\rangle$, and the oscillation frequency Ω_{B} is as follows:[25]

$$\Omega_{\text{B}} = \frac{-2J\Omega^2(-J\left(\alpha^{(1)}+\alpha^{(2)}\right)+\alpha^{(2)}\left(\alpha^{(1)}+\delta\right)+\alpha^{(1)}(\alpha^{(2)}-\delta))}{\left(\alpha^{(1)}+\delta\right)(\alpha^{(2)}-\delta)\delta^2}. \tag{2}$$

Here, Ω is the magnitude of the driving field. It is assumed that the driving field has a similar coupling strength with each qubit. When the length of the driving pulse is equal to a quarter of oscillation period $t = \pi/2\Omega_{\text{B}}$, this kind of pulse operation is defined as two-qubit logical gate $\sqrt{\text{bSWAP}}$. Setting the driving frequency at $\omega_d = 2\pi \times 7.1186$ GHz, the experimental result of $|00\rangle \rightarrow |11\rangle$ two-photon Rabi-like oscillation is obtained in this qubit–qubit coupling system, as shown in Fig. 7. It presents the variation of Rabi-like oscillations at different drive powers, and shows that the oscillation saturates at a value larger than the intermediate value. This is due to the Jaynes–Cummings readout method. Compared with the output signal of the ground state, when the system is excited, the amplitude of the output signal is much larger. As the oscillation satu-

ration value is larger than the intermediate value, it indicates that the population of the excited state is larger than that of the ground state. The system finally saturates in the steady states of all four states $|00\rangle$, $|01\rangle$, $|10\rangle$, and $|11\rangle$, instead of the mixture of two states $|00\rangle$ and $|11\rangle$.

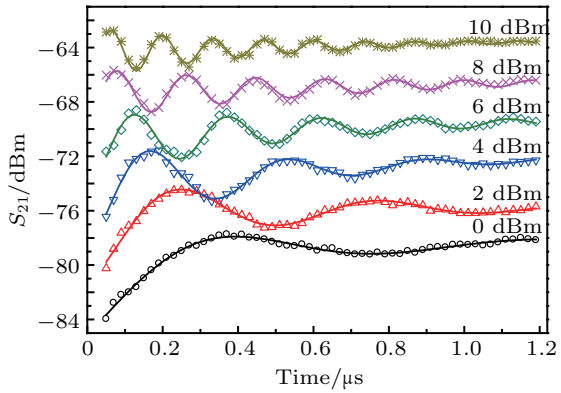


Fig. 7. (color online) The Rabi-like oscillations of the two-photon process $|00\rangle \rightarrow |11\rangle$ in different driving powers.

Taking the decoherence of Q1 and Q2 into account, the following function is used for fitting the two-photon Rabi-like oscillation:

$$S = a_0 + a_1 \times \mathrm{e}^{-t/T_{\mathrm{Rabi}}^{00-11}} \times \sin\left(\Omega_{\mathrm{B}} t - \frac{\pi}{2}\right) + a_2 \times \mathrm{e}^{-t/T_{Q1,Q2}}. \quad (3)$$

Here, $T_{\mathrm{Rabi}}^{00-11}$ is the decoherence time of the Rabi-like oscillation, while $T_{\mathrm{Q1,Q2}}$ is the decoherence time of each qubit. Based on this function, the fitting results are shown in Fig. 7. The blue and green curves correspond to the Rabi-like oscillation under the drive power 4 dBm and 6 dBm, respectively. The fitting curve matches well with the experimental data, and thus this function can be used to describe the two-photon process $|00\rangle \rightarrow |11\rangle$. From the fitting results, when the driving power is 4 dBm, the corresponding parameters are $T_{\mathrm{Rabi}}^{00-11} = 0.44$ μs, $T_{\mathrm{Q1,Q2}} = 0.91$ μs, and $\Omega_{\mathrm{B}} = 2\pi \times 3.39$ MHz. When the driving power is 6 dBm, the parameters are $T_{\mathrm{Rabi}}^{00-11} = 0.49$ μs, $T_{\mathrm{Q1,Q2}} = 0.97$ μs, and $\Omega_{\mathrm{B}} = 2\pi \times 4.03$ MHz. According to the fitting results, it has the relationship $T_{\mathrm{Rabi}}^{00-11} < T_{\mathrm{Q1,Q2}} < T_{\mathrm{Rabi}}^{(1)}$, $T_{\mathrm{Rabi}}^{(2)}$, which indicates noise has greater effects on the two-photon process. Due to the noise effects, the decoherence time of the two-photon process is shorter than the single qubit decoherence time. Another explanation involves the effect of the two-photon drive field. It may produce the ac-Stark effect on each qubit and make the spectrum shifted and broadened. Therefore, the decoherence time of the two-photon process becomes shorter.

4. Conclusion

To summarize, we have implemented the coupling system of two separated transmon qubits in a 3D cavity. The two qubits do not couple with each other directly. They indirectly interact by virtual-photon via cavity. Due to the coupling effect, by tuning the transition frequency of one qubit, avoided crossing spectrum is observed in the process of single photon transition $|00\rangle \rightarrow |10\rangle$ and $|00\rangle \rightarrow |01\rangle$. The degree of splitting reflects the qubit–qubit coupling strength $2J = 2\pi \times 29$ MHz. With ac-Stark effect, fast tuning of qubit transition frequencies is realized. By varying the ac-Stark driving power and frequency, the two qubits are tuned near resonance and the exchange of states is realized between the two qubits. A quarter swap period of the stark pulse corresponds to a two-qubit $\sqrt{\mathrm{iSWAP}}$ gate operation. Besides, applying a driving field with a driving frequency near $(f_{01}^{(1)} + f_{01}^{(2)})/2$ to this qubit–qubit coupling system, we have successfully performed Rabi-like oscillation of two-photon process $|00\rangle \rightarrow |11\rangle$, and a quarter period of the oscillation corresponds to $\sqrt{\mathrm{bSWAP}}$ gate operation.

Acknowledgment

We would like to thank Zhejiang Tianjingsheng Foundation, China, for student assistantships.

References

[1] Devoret M H and Schoelkopf R J 2013 *Science* **339** 1169
[2] Masoud Mohseni, Peter Read, Hartmut Neven, *et al.* 2017 *Nature* **534** 171
[3] Chow J M, Gambetta J M, Córcoles A D, *et al.* 2012 *Phys. Rev. Lett.* **109** 060501
[4] Barends R, Kelly J, Megrant A, *et al.* 2014 *Nature* **508** 500
[5] Hatridge M, Shankar S, Mirrahimi M, *et al.* 2013 *Science* **339** 178
[6] Zhong Y P, Li C Y, Wang H H, *et al.* 2013 *Chin. Phys. B* **22** 110313
[7] Vijay R, Macklin C, Slichter D H, *et al.* 2012 *Nature* **490** 77
[8] Reed M D, DiCarlo L, Johnson B R, *et al.* 2010 *Phys. Rev. Lett.* **105** 173601
[9] Jeffrey E, Sank D, Mutus J Y, *et al.* 2014 *Phys. Rev. Lett.* **112** 190504
[10] Barends R, Shabani A, Lamata L, *et al.* 2016 *Nature* **534** 222
[11] Gambetta J M, Chow J M and Steffen M arXiv: 1510.04375v1 [quant-ph]
[12] Kelly J, Barends R, Fowler A G, *et al.* 2015 *Nature* **519** 66
[13] Chow J M, Gambetta J M, Magesan E, *et al.* 2014 *Nat. Commun.* **5** 4015
[14] Reed M D, DiCarlo L, Nigg S E, *et al.* 2012 *Nature* **482** 382
[15] Lucero E, Barends R, Chen Y, *et al.* 2012 *Nat. Phys.* **8** 719
[16] Chen Yu, Neill C, Roushan P, *et al.* 2014 *Phys. Rev. Lett.* **113** 220502
[17] Neeley M, Bialczak R C, Lenander M, *et al.* 2010 *Nature* **467** 570
[18] DiCarlo L, Reed M D, Sun L, *et al.* 2010 *Nature* **467** 574
[19] Bialczak R C, Ansmann M, Hofheinz M, *et al.* 2010 *Nat. Phys.* **6** 409
[20] Ansmann M, Wang H, Bialczak R C, *et al.* 2009 *Nature* **461** 504
[21] Evan Jeffrey, Daniel Sank, Mutus J Y, *et al.* 2014 *Phys. Rev. Lett.* **112** 190504
[22] Majer J, Chow J M, Gambetta J M, *et al.* 2007 *Nature* **449** 443
[23] Sank D, Chen Z, Khezri M, *et al.* 2016 *Phys. Rev. Lett.* **117** 190503
[24] Mariantoni M, Wang H, Yamamoto T, *et al.* 2011 *Science* **334** 61
[25] Poletto S, Gambetta Jay M, Merkel Seth T, *et al.* 2012 *Phys. Rev. Lett.* **109** 240505